Local atomic and electronic structure in $LaMnO_3$ across the orbital ordering transition

Raquel A. Souza,[1,2] Narcizo M. Souza-Neto,[1,3] Aline Y. Ramos,[1,4,*] Hélio C. N. Tolentino,[1] and Eduardo Granado[1,2]

[1]*Laboratório Nacional de Luz Síncrotron - LNLS, P.O. Box 6192, 13084-971, Campinas, São Paulo, Brazil*

[2]*Instituto de Física Gleb Wataghin, IFGW - UNICAMP, Campinas, SP, Brazil*

[3]*Dept. de Física dos Materiais e Mecânica, DFMT-IF-USP, São Paulo, SP, Brazil*

[4]*Laboratoire de Minéralogie-Cristallographie de Paris, LMCP -UMR 7590 -CNRS, Paris, France*

(Dated: 2nd February 2008)

The local atomic disorder and the electronic structure in the environment of manganese atoms in $LaMnO_3$ has been studied by x-ray absorption spectroscopy, over a temperature range (300K to 870K) covering the orbital ordering transition ($\sim$710K). The Mn-O distances splitting into short and long bonds (1.95 and 2.15Å) is kept across the transition temperature, so that the MnO_6 octahedra remain locally Jahn-Teller distorted. Discontinuities in the Mn local structure are identified in the extended x-ray fine structure spectra at this temperature, associated to a reduction of the disorder in the super-exchange angle and to the removal of the anisotropy in the radial disorder within the coordination shell. Subtle changes in the electronic local structure also take place at the Mn site at the transition temperature. The near edge spectra show a small drop of the Mn $4p-$hole count and a small enhancement in the pre-edge structures at the transition temperature. These features are associated to an increase of the covalence of the Mn-O bonds. Our results shed light on the local electronic and structural phenomena in a model of order-disorder transition, where the cooperative distortion is overcome by the thermal disorder.

PACS numbers: 75.47.lx, 61.10.Ht, 71.90.+q

I. INTRODUCTION

The lanthanum manganite and its doped perovskite alloys $La_{1-x}A_xMnO_3$ (with A= Ca, Sr, Ba) have attracted much attention in the last decade, in large part due to the potential applications of the so called colossal magnetoresistance[1]. The unusual physical properties of these compounds arise from intricate interrelations between spin, charge and local structure. In spite of the large experimental and theoretical efforts of the scientific community many of these interrelations remain not elucidated. In the $LaMnO_3$ compound itself many questions remain to be addressed. At room temperature $LaMnO_3$ is an antiferromagnetic semiconductor and crystallize in an orthorhombic variant of the cubic perovskite structure space group *Pbnm*. The MnO_6 octahedra in $LaMnO_3$ are distorted due to the Jahn-Teller (JT) effects of the $Mn^{3+}(t_{2g}^3 e_g^1)$ and the $Mn-O$ distances are split into two groups. The manganese atoms are coupled ferromagnetically in the ab plane and antiferromagnetically along the c axis and an orbital ordering takes place. In the basal ab plane long and short $Mn-O$ bonds alternates. The apical and basal short bonds have different length (≈ 1.91Å and ≈ 1.97Å respectively), however this additional splitting is small for local probes such as real space high resolution diffraction [2, 3, 4] and extended x-ray absorption fine structure (EXAFS)[5, 6, 7]. The local radial distribution is thus seen as made of a single distance at $(Mn-O)_s \approx 1.94$Å, separated from the long distance long bond $(Mn-O)_l \approx 2.15$Å. $LaMnO_3$ undergoes a transition at $T^* \approx$710-750 K from the JT distorted orthorhombic phase to a high temperature nearly cubic phase [8]. The space group *Pbnm* remains the same in both phases, but the cell distortion is nearly removed and the orbital ordering disappears in the high temperature phase. The transition is accompanied by abrupt changes in the electrical resistivity, thermoelectric power and Weiss constant [9].

At the local scale two scenarios may be proposed: symmetrization of the distorted octrahedra MnO_6 or an order-disorder transition, where the local distortion is maintained. From thermodynamic calculations it has been shown [10] that the thermal energy at T^* is small with respect to the gain associated to the lift of the e_g levels degeneracy, so that this transition will hardly correspond to a removal of the octahedral distortion. The transition would happen as an order-disorder transition in the sequence of the distorted octahedra. Experimentally, two early works from Raman spectroscopy [11] and from the analysis of the overall disorder in the EXAFS data across T^* [12], supported the hypothesis of the upkeep of the local JT distortion. On the other hand the hypothesis that the local JT distortion may vanish and the $Mn-O$ distances collapse, was sustained by the work in thin

*Electronic address: aramos@lnls.br

$LaMnO_3$ films [13]. The two distances found by the fitting procedure [13] collapse into a single one above a given temperature, in a similar way as the cell parameters. More recently, Sanchez et al.[14] have reached opposite conclusions from their x- ray absorption study in $LaMnO_3$ polycrystals.

There have been various works using X-ray absorption spectroscopy (XAS), shedding light on the nature of the Jahn-Teller distortion, electronic states, thermal behavior and disorder in manganites[5, 6, 7, 12, 14, 15, 16, 17, 18, 19, 20, 21]. The thermal and the structural disorder enter equivalently in the theory and in the data analysis where the overall disorder is usually expressed by a Debye Waller-like factor (DWF). The thermal disorder depends on the dynamical properties of the lattice. It presents a smooth continuous increase with the temperature that can be modeled using models of correlated vibrations [22]. The structural local disorder accounts for bonds length dispersion and site distortions that, in the absence of structural transition, are temperature independent. At high temperatures, the EXAFS signal is strongly damped by the thermal disorder. The limited available analysis range reduces the R-resolution and closely correlated fitting parameters cannot always been unambiguously resolved[5]. In addition, the structural disorder associated to the long and the short $Mn-O$ bonds are significantly different [6, 7] and the thermal behavior of the DWF may not be correlated. To avoid misfits in the choice of fixed or correlated parameters, qualitative methods using an alternative way of data handling may be useful, prior to the application of the fitting procedure. The phase derivative method, based on the analysis of the beat stemming from the combination of two close frequency sinusoids, has proved in several complex systems its usefulness as a diagnostic tool[23, 24, 25]. This method, by characterizing the occurrence of a distance splitting, should be especially useful to identify possible collapse of this splitting as the temperature is increased. With the support of this evidence, the EXAFS fitting analysis should then be specially focused on the behavior of the disorder related Debye Waller-like term.

X-ray absorption near edge spectroscopy (XANES) has been shown to be very sensitive to the various degrees of freedom governing the electronic properties of manganite compounds, such as local atomic distortion, charge transfer in the $Mn-O$ bond, or local magnetic ordering [5, 6, 7, 17, 18, 19, 20, 21]. The temperature dependence of XANES spectra in $LaMnO_3$ has been the object of some reports in the literature[18, 19, 20], but most of them are related to the thermal behavior of this compound around the magnetic ordering temperature ($\sim$140K). It can be expected that temperature dependence of XANES spectra across the orthorhombic to cubic transition may shed more light on the modification in the local atomic and electronic structure at the site of the Mn^{3+} ions.

We address here the issue of the temperature dependence of the local distortion around Mn^{3+} ions in $LaMnO_3$ with a complete set of EXAFS and XANES data, collected below and above T^*. At this temperature some discontinuities are observed in both EXAFS and XANES range data. In the EXAFS range, the Jahn-Teller distance splitting still exists within the coordination shell even above the transition, but modification in the disorder can be identified. At low temperature the static disorder associated to the long bond $(Mn-O)_l$ is about three times larger than the disorder associated to the short bond $(Mn-O)_s$. As the temperature increases the overall disorder associated to the short bond is rapidly dominated by the thermal contribution whereas the structural term is still dominant for the long bond. Around T^* these terms become of the same order and the thermal disorder is likely to be dominant for all the apical and basal bonds. We conclude then that the tetragonal distortion is preserved across T^*, in agreement with an order-disorder character for the transition. We point out that this transition takes place when the relative displacement of the atoms along the long and short bonds becomes of the same order, turning the average radial disorder isotropic and allowing the bond length to vary independently. In the XANES range, the weak but significant discontinuities observed across T^* are associated to an increase of the covalent character of the $Mn-O$ bonds.

II. EXPERIMENTAL

The Mn-K edge EXAFS spectra were collected on a powder of $LaMnO_3$ synthesized by the solid state reaction method. The sample shows an orthorhombic to cubic transition at $T^* \sim 710K$. Details of the synthesis method, the structural characterization and magnetic of the sample have been published elsewhere [11]. The temperature dependent x-ray absorption measurements were performed at LNLS D04B-XAS1 beamline [26] in the transmission mode. A fine grained powder sample of $LaMnO_3$ was pressed between two thin beryllium windows and placed into an electrical furnace with low vacuum ($< 10^{-3}$Torr). EXAFS and XANES data were collected at increasing temperature from 300K to 870K. Then the temperature has been decreased and the XAS spectra have been collected again at some temperature points and compared to those previously collected. Using this procedure we can certify that the sample had not been oxidized during the high temperature measurements. In addition we verify with this procedure the perfect reproducibility of the subtle features in the XANES spectra. The EXAFS data were collected up to k_{max}=12.5Å^{-1}. This data range limits the minimum difference between two close distances that can be resolved in the EXAFS analysis to the value $(\delta R)_{\min}$= 0.13Å. The two distances at 1.91Å and 1.97Å are seen as one unique distance $(Mn-O)_s \approx 1.94$Å, easily resolved from the long distance $(Mn-O)_l \approx 2.15$Å (δR= 0.21Å). The experimental resolution for the XANES experiments was about 1.5eV. The simultaneous collection of XANES metal foil reference spectra enables the eventual correction of small energy shift due to thermal effects in the optics of the beam line. After background subtraction the spectra

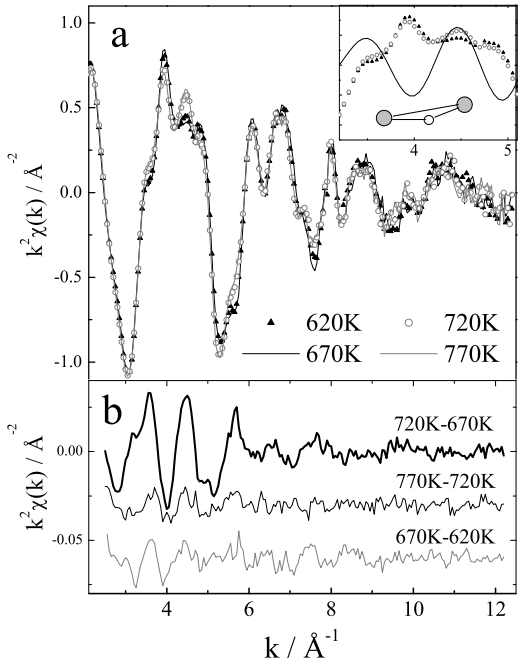

Figure 1: EXAFS signal (a) and difference spectra (b) below, above and across the transition temperature T^* .The inset is a zoom of the first EXAFS oscillation showing the simulation of the 3-leg MS contribution, in phase with main additional structure above the transition.

were normalized in the range 150-250eV above the edge. The features in the XANES spectra can then be compared in intensity, and in position with a sensitivity as low as 0.1eV.

The EXAFS oscillations were extracted following standard procedure[27]. The signal corresponding to the oxygen coordination shell is selected by Fourier filtering. A first analysis has been made using the phase derivative (PD) method. This method is based on the exploration of the modulation in the EXAFS signal occurring when the contributions of two close shells separated by δR are combined. For close shells with the same backscattering atom, this modulation results in a minimum in the total amplitude and an inflexion in the total phase of the EXAFS signal, at $k = k_B$ given by $k_B \sim \pi/2\delta R$[23, 24, 25]. The presence of a beat is widely used to identify the occurrence of close shells. Due to the approximations involved, $\delta R_B = \pi/2k_B$ does not give exactly the bond length separation, however any relative modification in this separation will be detected by a shift in the beat position. The second analysis consisted in the application of the conventional fitting procedure constraining the parameters using the information obtained from the *PD* method. In the fitting procedure, the number of free parameters is limited to $n \approx 7$, by the useful range and the interval corresponding to the selected signal in the real space.

III. RESULTS AND DISCUSSION

The k^2-weighted χ(k) spectra [$\chi(k) * k^2$] for selected temperatures below and above the cell ordering temperature $T^*(\sim 710K)$ are shown in the Fig.1a. On the Fig.1b, we report the difference EXAFS spectra for measurement at temperature differing by 50K, just below, just above, and across the transition. Subtle modifications are observed across T^*. The high frequency of these modifications indicates that they are associated to higher shells or multiple scattering (MS) effects. We would like to call attention to the additional feature appearing around k =4.5Å^{-1}in the EXAFS spectra (Fig.1a). This feature is common, with different scale of intensities, to all reported EXAFS spectra of manganite compounds, but is absent in $LaMnO_3$ below T^* [5, 6, 7, 14, 15]. Aiming to determine the exact origin of this contribution, we perform *ab initio* simulations in MS expansion, using the Feff7 code[28, 29]. Different clusters were built, using the crystallographic structure of *Pbnm* and $R\overline{3}C$ doped compounds. A path by path study allowed the identification of the additional contribution above T^* as being mainly due to 3-leg MS paths involving two neighboring Mn atoms and their common oxygen (Fig.1a, inset). The contribution of this path increases with increasing the superexchange angle (tilt angle) Mn-O-Mn, as well as with the reduction of angular disorder. This contribution is clearly revealed, in the Fourier transform (FT) of the EXAFS signal across T^* (Fig. 2). Apart from other modifications, discussed below, a large peak around 3Å corresponding to that MS contribution shows up in the difference signal (Fig. 2b). As neutron diffraction studies[8] do contain any report of an anomalous behavior in the average tilt angle, we may conclude that the enhancement of

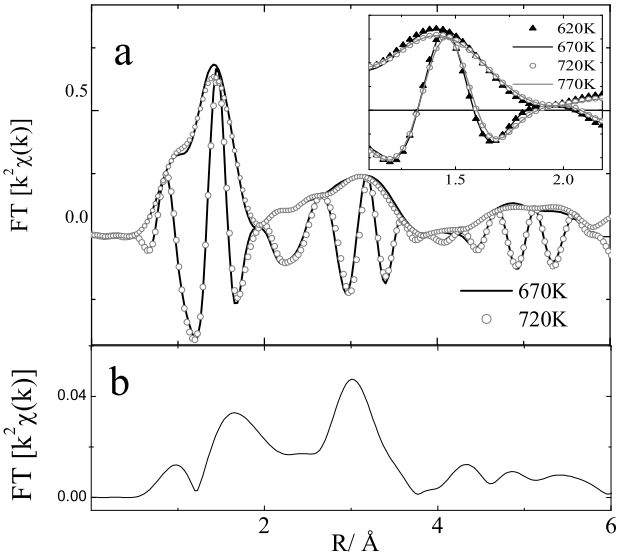

Figure 2: (a) Fourier transform of the EXAFS signal across T^* (modulus and real part). Inset : detail of the first peak corresponding to the coordination shell. Subtle but reproducible changes are observed for temperature below and above the transition temperature. (b) Modulus of the Fourier transform of the difference EXAFS signal across T^*, showing the two differential contributions around 3 and 1.8 Å.

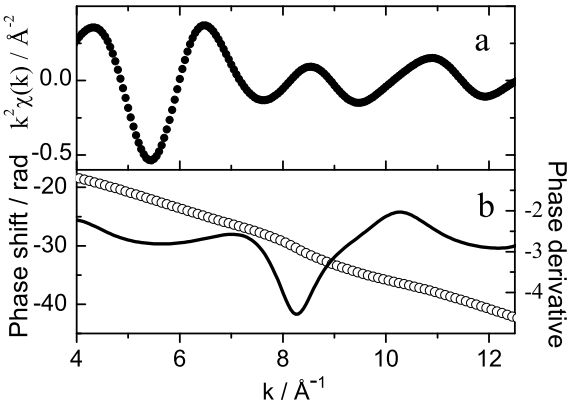

Figure 3: a. Back Fourier transformed signal of the coordination shell at room temperature. b.Total phase shift and derivative: the minimum of the curve defines the beat position k_B.

the MS contribution at $T^*$is more likely related to a reduction of the average angular disorder.

A closer view of the first peak in FT corresponding to the contribution of the coordination shell (Fig.2a, inset) reveals small but significant modifications occurring within the MnO_6 octahedra, across the transition. The shape of the signal is not notabily affected, but we observe a small drop in the height of the peak (at $\sim$1.3Å) and a discontinuity in the thermal sequence, clearly seen in the real FT component, in the high R side of the peak (at $\sim$1.8Å) , associated to the long bond contribution [7]. The Fourier transform of the difference spectra across T^*(Fig.2b) shows a peak around 1.8 Å, confirming the occurrence of a structural modification within the coordination shell. As already pointed out, the thermal damping may smooth and screen part of the real effects, so that a thorough analysis is necessary to determinate the extent of modification of the local atomic organization.

The *PD* method was applied in the analysis of this coordination shell contribution, first for the room temperature (RT) spectrum, where the local structure is already well established. The EXAFS signal was back Fourier transformed in the R-range 0.7Å to 2.1Å (fig.3a). A minimum in the total amplitude (fig.3a) and an inflexion point in the total phase (fig.3b) are observed at $k_B = 8.3$Å^{-1}. This beat position corresponds to a value $\delta R_B = \pi/2k_B = 0.19$Å, in good agreement with bond length separation obtained from crystallographic data (δR= 0.21Å). The small difference, most likely due to the approximations involved in the *PD* method[23], is commonly reported [24, 25] and does not affect the precision in the relative modification of this separation, that should be revealed by a shift in the beat position. Identical procedure of the phase extraction have been applied to the EXAFS spectra in the whole temperature range, leading to a beat position value comprised between 8.1 and 8.5Å^{-1}(Fig.4a). A

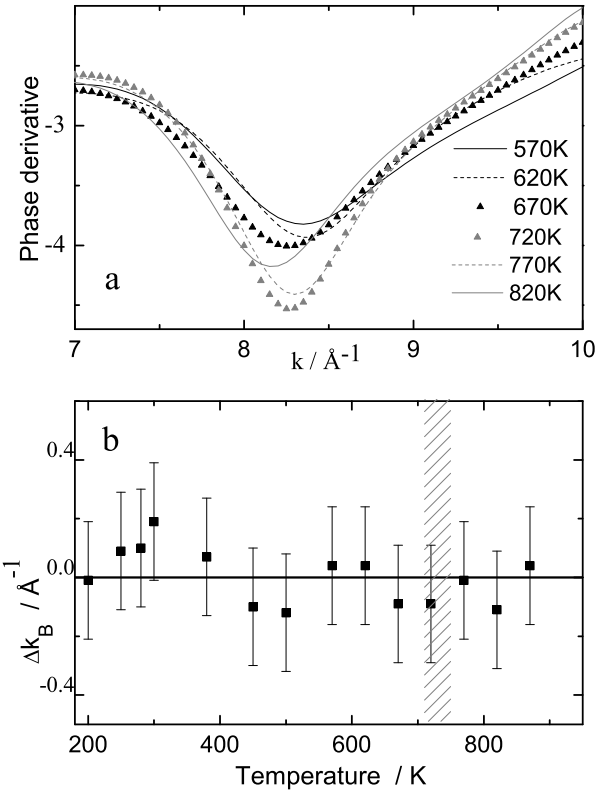

Figure 4: a. Total phase shift derivative: the minimum of the curve defines the beat position k_B. b. Variation of the k_B value with the temperature. The domain where orthorhombic to cubic transition takes place is marked by the hatched area.

relative error of 5% has been estimated from the mean square deviation for spectra collected at the same temperature. Within this error bar the same value of k_B is obtained over the whole temperature range, showing that the bond length splitting is kept constant across T^* (Fig.4b).

A two-shell fit in k-space is then performed using theoretical amplitude and phase functions generated using FEFF7 code [28, 29] from the crystallographic *Pbnm* structure of $LaMnO_3$. The number of first neighbors were fixed ($N_1 = 4$ for the short $(Mn-O)_s$ bonds and $N_2 = 2$ for the $(Mn-O)_l$ long bonds) and the value of the amplitude reduction factor S_0^2 was determined from RT spectra and then fixed for the analysis of the spectra at other temperatures. Figure 5 shows the results of the fit. We note that the $Mn-O$ distances remain almost constant through T^* at values close to those known for $LaMnO_3$ at RT : $(Mn-O)_s = 1.93$Å and $(Mn-O)_l = 2.15$Å, confirming that there is no collapse of these distances across the transition.

As concerns the disorder, the study of the Debye-Waller term brings about some interesting observations. As already been pointed out in previous XAS studies [6, 7], the disorder associated to the long and the short bonds at room temperature are quite different. According to the prediction of Goodenough [30] about the character of the Mn-O bonding, the short $(Mn-O)_s$ bonds are stable bonds with semicovalent character, while the long $(Mn-O)_l$ distance corresponds to a weaker ionic bonding. The static radial disorder associated to the ionic long bonds is large ($\sigma = 0.07$ Å) and keeps almost the same value over the whole temperature range below T^* . The radial disorder associated to the short bonds is about three times smaller at room temperature, in agreement with the results reported in the literature. The evolution of this factor is thermally driven, well accounted by a simple correlated model for the thermal vibrations[22]. The temperature found for the Einstein model is $\Theta_E \sim 680K$ (Fig.5), in agreement with the high Debye temperatures ($\Theta_D \sim 3/2\Theta_E \sim 1000K$) already reported in perovskites compounds[2, 18]. The DWF associated to long bond is almost temperature independent up to values close to T^*. At this temperature we observe a small drop in this factor, partially screened by the error on the determination of σ^2. We should point out that at this temperature the DWF associated to short and long bonds assume essentially the same values. Above T^* both factors seem to follow a simple thermal behavior, in the continuity of the low temperature behavior of the short bond DWF.

The small drop in the long bond DWF is consistent with the small discontinuity in the long bond -related side in the FT (Fig.2). As the distances are kept constant and the DWF associated to the short bond increases continuously, it should be related to the drop in the height of the peak in the FT across the transition. We should emphasize that the DWF in EXAFS only accounts for radial disorder, *i.e.* the relative variation in the Mn and O positions, projected along the bond axis. In the basal plane, all

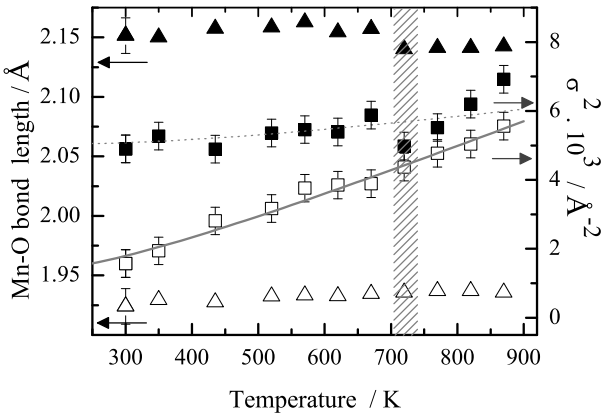

Figure 5: Mn-O bond lengths (triangles, left scale) and associated DWF (square, right scale). The open symbols and plain symbols correspond to short and long lengths respectively. For seek of clarity the error bars in the bond lengths, almost constant over the temperature range, have been shown only for room temperature. The plain line is the fit of the thermal disorder using the correlated Einstein model. The dot line is only a guide for the eyes. A small drop of the long bond DWF is observed at T^*(hatched area). At this temperature the DWF of the short and long bonds are equalized.

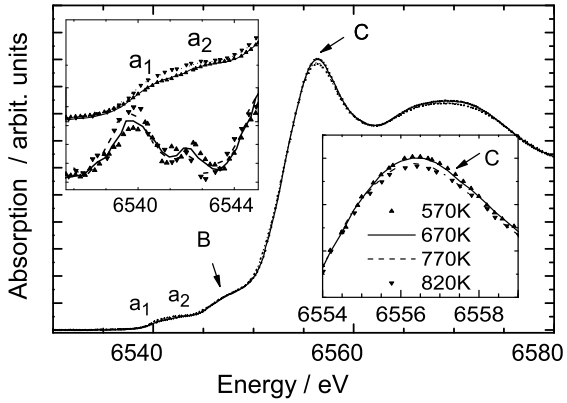

Figure 6: XANES spectra across the orbital ordering temperature ($\sim 710K$). The insets are close views showing the subtle discontinuities in amplitude. Left inset : preedge region and corresponding absorption derivative. Right inset: main feature C.

the Mn-O-Mn linkages are composed of a long and a short bond. The longitudinal variation of $(Mn-O)_l$ length should then be accommodated by flattening and unbending the Mn-O-Mn angle. The resulting transverse accommodation has a limited projection on the $(Mn-O)_s$ bond, and is not "seen" in the radial disorder term. Additionally, the accommodation through the Mn-O-Mn angle yield to destructive interferences in the different multiple scattering contributions of the almost linear 3-leg MS paths (Fig.1a- insert) and limits the total contribution to the EXAFS signal. Around T^* the radial DWF of $(Mn-O)_s$ bonds becomes of the same order as that of $(Mn-O)_l$ bonds and the variations of the short and long bonds are almost decorrelated. The two terms follow then similar thermal behaviors. The Mn-O-Mn angle is no more so strongly involved in the accomodation the bond vibrations and the contribution of the multiple scattering path involving the two adjacent Mn and their common O increases. The reduction of the angular distortion favors an increase of the hybridization between the Mn 3d and O 2p orbitals.

The XANES spectra across the transition (570K to 820K) are shown in Fig.6. The spectra exhibit the features already reported in $LaMnO_3$ [17, 18, 19, 20, 21]. The two pre-edge peaks a_1 and a_2 (6540.0 and 6542.4eV) arise essentially from 1s-4p dipole allowed transitions of Mn 3*d* character. They account for the hybridization of the Mn 4*p* orbitals with the Mn 3*d* orbitals on neighboring Mn ions, either directly or via O atoms [31, 32]. In reduced symmetry due to the local Jahn-Teller distortion of the MnO_6 octahedra, the $1s \rightarrow 4p$ transition on Mn site is split into separable components close to the onset (shoulder B) around 6546eV and at the top of the rising edge (C main peak) in the region 6550-6560eV where lies most of the spectral strength [18]. There is no energy shift in the XANES over the whole temperature range, in agreement with the absence of significant modification in the average coordination distance. It has been recently invoked [33] that a charge disproportionation for the Mn ions could happen at the transition temperature. However this would result in a splitting in the rising edge that has not been observed. Drastic changes in the charge disproportionation should then be excluded. The top of the main feature C measures the

net $4p-$hole count. Up to the transition temperature the intensity of this C peak decreases very slowly and continuously when the temperature increases as a consequence of the increase of the thermal disorder. At the transition a small additional drop in the maximum peak height takes place (Fig.6, inset). We should remind that the experimental procedure based on the collection of the XAS data twice, both at increasing and decreasing temperature, assure us the perfect reproducibility of the XANES features. Small changes in the intensity of the features, especially in the maximum peak height, are not experimental artifacts. An additional drop in the hole count is then observed across the transition. It accounts for an additional non-thermal increase of the delocalization of the e_g electrons, through a band effect associated to the increase of the average Mn-O bond covalence[31]. Correlatively, subtle but reproducible modifications are observed in the preedge domain (Fig.6 inset). Alterations in the spectral weight of these features are currently associated to modification in the distribution of e_g majority and (e_g t_{2g}) minority states [18]. In the present case we do not observe spectral transfer from one to the other features, but the simultaneous enhancement of the two features. We associate this enhancement to an increase of the hybridization between the Mn $4p$ orbitals and the Mn $3d$ orbitals on neighboring atoms. This is consistent with a reduction of the disorder in the superexchange angle deduced from EXAFS analysis. The delocalization of the e_g electrons due to the thermal disorder partly overcome the localization associated to the ionic bonds and should be related to the reported drop in the resistivity at the orbital ordering temperature[9, 21].

IV. CONCLUSIONS

We reported a XAS study of the local atomic and structural modifications around the manganese atoms in $LaMnO_3$ across the orbital ordering transition T^*. The Jahn-Teller splitting into long $(Mn-O)_l$ and short $(Mn-O)_s$ bonds within the MnO_6 octahedra is kept in the high temperature phase. We observe that significant electronic and structural changes are taking place across this transition at the Mn site. We show that the structural modifications correspond to a change in the accommodation of the local thermal disorder related to vibrations of the $Mn-O$ bonds. We point out that the orbital ordering transition takes place when the relative displacement of the atoms along the long and short bonds becomes of the same order. Below T^*, the radial thermal disorder appears to be mostly accomodated by bending of the tilt angle Mn-O-Mn among adjacent octahedra. Above T^*, the Mn-O-Mn angle are flattened and strengthened and the average radial disorder becomes isotropic, allowing a complete decorrelation of the bond length variations. Subtle electronic modifications at the Mn sites also take place : a small drop in the 4p counts and a small enhancement of the hybridization between 4p and 3d orbitals are observed across the transition. These modifications are associated to an increase of the average covalent character of the $Mn-O$ bonds.

This work is partially supported by LNLS/ABTLuS/MCT. RAS acknowledges the PIBIC/CNPq. AYR acknowledges the grant from CNPq/PCI

[1] A. J. Millis, Nature **392**, 147 (1998).
[2] T. Proffen, R. Francesco, S. Billinge, E. Brosha, and G. Kwei, Phys. Rev. B **60**, 9973 (1999).
[3] S. Billinge, T. Proffen, V. Petkov, J. L. Sarrao, and S. Kycia, Phys. Rev. B **62**, 1203 (2000).
[4] D. Louca, E. Brosha, and T. Egami, Phys. Rev. B **61**, 1351 (2000).
[5] C. H. Booth, F. Bridges, G. Kwei, J. M. Lawrence, A. L. Cornelius, and J. Neumeier, Phys. Rev. B **57**, 10440 (1998).
[6] G. Subías, J. García, J. Blasco, and M. Proietti, Phys. Rev. B **58**, 9287 (1998).
[7] T. Shibata, B. Bunker, and J. F. Mitchell, Phys. Rev. B **68**, 024103 (2003).
[8] J. Rodriguez-Carvajal, M. Hennion, F. Moussa, A. Moudden, L. Pinsart, and A. Revcolevschi, Phys. Rev. B. **57**, R3189 (1998).
[9] J.-S. Zhou and J. Goodenough, Phys. Rev. B. **60**, R15002 (1999).
[10] A. Millis, Phys. Rev. B. **53**, 8434 (1996).
[11] E. Granado, J. A. Sanjurjo, C. Rettori, J. Neumeier, and S. Oseroff, Phys. Rev. B **62**, 11304 (2000).
[12] E. Araya-Rodriguez, A. Y. Ramos, H. C. N. Tolentino, E. Granado, and S. Oseroff, J. Magn. Magn. Mat. **233**, 88 (2001).
[13] J. Song, J. Park, K. Leee, J. Lee, and Y. Jeong, Phys. Rev. B. **66**, 020407 (2002).
[14] M. Sánchez, G. Subías, J. García, and J. Blasco, Phys. Rev. Lett. **90**, 045503 (2003).
[15] T. A. Tyson, J. M. de Leon, S. D. Conradson, A. R. Bishop, J. J. Neumeier, H. Röder, and J. Zang, Phys. Rev. B **53**, 13985 (1996).
[16] A. Lanzara, N. Saini, M. Brunelli, F. Natali, A. Bianconi, P. Radaelli, and S. Cheong, Phys. Rev. Lett. **81**, 878 (1998).
[17] M. Croft, D. Sills, M. Greenblett, C. Lee, S.-W. Cheong, K. Ramanujachary, and D. Tran, Phys. Rev. B **55**, 8726 (1997).
[18] F. Bridges, C. H. Booth, G. Kwei, J. Neumeier, and G. Sawatzky, Phys. Rev. B **61**, R9237 (2000).
[19] F. Bridges, C. H. Booth, M. Anderson, G. Kwei, J. Neumeier, J. Snyder, J. Mitchell, J. Gardner, and E. Brosha, Phys. Rev. B **63**, 214405 (2001).
[20] Q. Qian, T. A. Tyson, C.-C. Kao, M. Croft, S.-W. Cheong, and M. Greenblatt, Phys. Rev. B **62**, 13472 (2000).
[21] Q. Qian, T. A. Tyson, S. Savrassov, C.-C. Kao, and M. Croft, Phys. Rev. B **68**, 014429 (2003).
[22] E. Sevillano, H. Meuth, and J. J. Rehr, Phys. Rev. B **20**, 4908 (1979).

[23] G. Martens, P. Rabe, N. Schwentner, and A. Werner, Phys. Rev. Lett. **39**, 1411 (1977).
[24] H. Jaffres, P. L. Fevre, H. Magnan, A. Midoir, D. Chandesris, L. Ressier, A. Schuhl, F. N. V. Dan, M. Goiran, J. P. Peyrade, et al., Phys. Rev. B. **61**, 14628 (2000).
[25] D. Jiang, E. Crozier, and B. Heinrich, Phys. Rev. B **44**, 6401 (1991).
[26] H. C. N. Tolentino, A. Y. Ramos, M. C. M. Alves, R. A. Barrea, E. Tamura, J. C. Cezar, and N. Watanabe, J. Synchrotron Rad. **8**, 1040 (2001).
[27] D. C. Koningsberger and R. Prins, eds., *X-Ray Absorption: Principles, Applications, Techniques of EXAFS, SEXAFS and XANES*, vol. 92 of *Chemical Analysis* (John Wiley and Sons, 1988).
[28] J. J. Rehr, J. M. de Leon, S. Zabinsky, and R. C. Albers, J. Am. Chem Soc. **113**, 5135 (1991).
[29] J. J. Rehr, R. C. Albers, and S. Zabinsky, Phys. Rev. Lett. **69**, 3397 (1992).
[30] J. Goodenough, Phys. Rev. **100**, 564 (1955).
[31] I. S. Elfimov, V. I. Anisimov, and G. A. Sawatzky, Phys. Rev. Lett. **82**, 4264 (1999).
[32] L. Hozoi, , A. de Vries, and R. Broer, Phys. Rev. B **64**, 1651104 (2001).
[33] J.-S. Zhou and J. Goodenough, Phys. Rev. B. **68**, 144406 (2003).